Geophys. J. Int. (2005) **163,** 1025–1038 doi: 10.1111/j.1365-246X.2005.02767.x

Temperature dependence of shear wave attenuation in partially molten gabbronorite at seismic frequencies

Fabrice R. Fontaine,[1] Benoit Ildefonse[1] and Nickolai S. Bagdassarov[2]

[1] *Laboratoire de Tectonophysique, ISTEEM, CNRS/Université Montpellier II,* F-34095 *Montpellier cedex* 5, *France. E-mail: fontaine@dstu.univ-montp2.fr*
[2] *Institut für Meteorologie und Geophysik, J. W. Goethe Universität Frankfurt, Feldbergstrasse* 47, D-60323 *Frankfurt/Main, Germany*

Accepted 2005 July 29. Received 2005 July 26; in original form 2004 June 1

SUMMARY

Torsion oscillatory deformation experiments have been performed at high temperatures (600–1170°C) and over a wide range of low frequencies (20–2.10^{-3} Hz) on fine-grained gabbronorite samples from the Oman ophiolite in order to determine the shear wave attenuation as a function of temperature and melt fraction. The specimens have a small and uniform grain size (0.25–0.3 mm) and do not contain secondary, hydrated minerals. Measurements of internal friction (Q^{-1}) were performed using a forced oscillatory torsion apparatus at small strains ($\sim 10^{-7}$), and with increasing small temperature steps to reduce thermal microcracking. The general dependence of Q^{-1} to frequency is $Q^{-1} \propto \omega^{-\alpha}$, where ω is the angular velocity of forced oscillations and α is an empirical exponent. Below the melting temperature ($\sim$1050°C), α has average values of $\sim$0.15 at low frequency ($\leq$0.5 Hz) and 0.06 at higher frequency. Above the melting temperature, α has average values of $\sim$0.22 at low frequency and -0.02 at higher frequency. This frequency dependence of Q^{-1} is attributed to a viscoelastic behaviour due to the diffusion controlled grain boundary sliding, and partially to the squirt flow of the melt-phase wetting grain boundaries. The onset of melting is associated with a markedly higher Q^{-1} and a stronger dependence of Q^{-1} on temperature. The melt-related mechanical dissipation process could be a melt squirt flow. The characteristic frequency for the melt squirt flow is $\omega_m \sim$ 0.15–300 Hz when the melt pocket aspect ratio is $\sim 10^{-3}$–10^{-2}. Around the melting temperature the internal friction can be approximated by an experimental power law $Q^{-1} = A \cdot [\omega^{-1} \cdot d^{-1} \cdot \exp(-E_a/RT)]^{\alpha}$ with $\alpha \sim 0.08$, $A = 34.72\ \mathrm{s}^{-\alpha}\ \mu\mathrm{m}^{-\alpha}$ and $E_a \sim 873\ \mathrm{kJ\,mol}^{-1}$.

Key words: attenuation, gabbro, laboratory measurement, partial melting, torsion deformation.

1 INTRODUCTION

The experimental measurements of internal friction at seismic frequencies on crystal-melt aggregates are important for the understanding of seismological anomalies of high seismic wave attenuation in partially molten regions. Various experiments on partially molten rocks at seismic frequencies have been conducted during the last two decades (e.g. Berckhemer *et al.* 1982; Kampfmann & Berckhemer 1985; Gribb & Cooper 1998; Jackson *et al.* 2000; Bagdassarov 2000). Although a substantial progress has been achieved in the characterization of Q^{-1}, the sensitivity of Q^{-1} to the presence of a melt phase remains poorly constrained. The primary objective of this work is to provide a new data set on Q^{-1} for a partially molten gabbroic rock at seismic frequencies and to characterize the effect of the melt phase on the internal friction. The questions to be addressed in this study are:

(i) Can the temperature dependence of Q^{-1} be described by an Arrhenius type of equation in the temperature range of melting?

(ii) What is the effect of progressive partial melting on the distribution of the melt phase in the intergranular space, on the average size of crystal grains, and on the temperature dependence of seismic wave attenuation?

A microgabbronorite from the Oman ophiolite was selected for the experiments because the rock sample displays a uniform grain size (0.25–0.3 mm) and does not contain any secondary hydrated minerals. Boudier *et al.* (2000) have shown the relatively common occurrence and the localization of gabbronorites in the crustal section of the Oman ophiolite.

The measurements of the internal friction on the microgabbronorite samples were performed at low frequency (20–2.10^{-3} Hz) and atmospheric pressure. After the experiments, samples were studied using optical and scanning electron microscopes to estimate the melt fraction and topology. This set of experiments allows us to

(i) determine the internal friction related to the presence of melt,

(ii) discuss the possible mechanism of attenuation related to the presence of melt and

(iii) document the presence and location of melt in the samples.

2 BACKGROUND

The non-elastic behaviour of solids in which a material demonstrates two different responses to applied stresses, an instantaneous and a time-delayed response, was called 'anelasticity' by Zener (1948). Zener anelasticity is a restricted form of the general linear viscoelastic theory. A viscoelastic behaviour is characterized by a continuous change from elastic behaviour at high frequencies/low temperatures to viscous behaviour at low frequencies/high temperatures. Seismic wave attenuation is a characteristic of anelastic or viscoelastic properties of rocks composing the Earth. Two types of seismic attenuation, which are difficult to distinguish, are classically defined: intrinsic attenuation and scattering (extrinsic) attenuation. Tselentis (1998) showed that for seismic body waves the regional scattering attenuation is negligible compared with intrinsic attenuation of rocks. In this laboratory study only intrinsic attenuation is considered.

The dissipation of shear strain energy Q^{-1}, is defined as

$$Q^{-1}(\omega) = \frac{J_2(\omega)}{J_1(\omega)} = \tan\varphi(\omega), \quad (1)$$

where $J_1(\omega)$ and $J_2(\omega)$ are the real and imaginary parts of the complex compliance $J(\omega)$, respectively, $\varphi(\omega)$ is the phase delay between the applied torque and the resultant angular strain of the sample and ω is the frequency of oscillations (Nowick & Berry 1972).

Q^{-1} is related to the energy dissipated per a cycle of deformation (e.g. Findley *et al.* 1976), defined as $\Delta W/W$ where ΔW is the energy loss per cycle of oscillation of a given amplitude, and W is the maximum energy which the system can store for a given amplitude. The relative energy losses E of a viscoelastic material per oscillation cycle is

$$E = \frac{\Delta W}{W} = 2\pi \sin\varphi. \quad (2)$$

The approximation $\sin\varphi \approx \tan\varphi \approx Q^{-1}$ is possible, when φ is small, and Q^{-1} represents the dissipation or attenuation coefficient of the seismic energy. A maximum error of 5 per cent is obtained from this approximation when $Q^{-1} \leq 0.3$, and in the literature Q^{-1} is known as an internal friction coefficient.

Numerous mechanisms of internal friction have been inferred for attenuation in rocks (e.g. Nowick & Berry 1972; Guéguen *et al.* 1981; Karato & Spetzler 1990; Bagdassarov 2000; Jackson 2000), including point defects, dislocation pinning, grain boundary sliding, diffusion at grain boundaries, squirt flow, viscous flow, and thermoelasticity.

3 SAMPLE DESCRIPTION

In the present experiments a fine-grained gabbronorite from the Oman ophiolite (sample 97OB1, from the upper gabbro section in the Sumail massif) have been used because of its small and uniform grain size (250–300 μm), and because the rock sample does not include any secondary, hydrated minerals. A small amount of cracks (0.5–1 per cent of the surface in thin sections) is present in the initial sample. These cracks are mostly intergranular, and 2-μm-thick disks (aspect ratio $\sim$1/150) approximate their geometry. At low temperatures and with low heating rate the pre-existing crack come into contact with each other, and the grain boundaries may widen due to differential thermal expansion (Johnston & Toksöz 1980). The contribution of cracks may result in a decrease of contact surfaces; which would reduce dissipation due to a sliding-friction-like mechanism (Johnston & Toksöz 1980). We assume that at high temperature the main contribution of these initial cracks on dissipation occurs through a melt squirt flow (Mavko & Nur 1975; Schmeling 1985). We have estimated the potential effect of melt-filled initial cracks on dissipation with a numerical model of squirt flow (Mainprice & Ildefonse, private communication, 2005). We found that the contribution of flat initial cracks to Q^{-1} remains lower than 0.01, whatever the crack aspect ratio (from 1 to 0.01). The grain size is small enough compared to the sample size, so that the studied medium can be considered as homogeneous at the measurement wavelengths (which are 0.38 km at 10 Hz and 380 km at 0.01 Hz). The number of wavelengths along the sample length (20–33 mm) is in the range 5.26×10^{-5}–8.68×10^{-5} at 10 Hz and in the range 5.26×10^{-8}–8.68×10^{-8} at 0.01 Hz (e.g. Aki & Richards 1980).

Our gabbronorite sample comprises 55 per cent plagioclase (An92), 31 per cent diopside, 14 per cent enstatite and displays a mosaic texture (Fig. 1). It has polygonal plagioclase, planar to curviplanar grain boundaries, 120° triple junctions and equigranular grains, which are the expression of a textural equilibrium (e.g. Hunter 1987). Microprobe analyses for each mineralogical phase are given in Bagdassarov (2000). Mg numbers, defined as molar $Mg/(Mg+Fe_T)^*100$, where Fe_T equals to the total iron content, are between 75.3 and 85.6 for orthopyroxenes and 77.6 and 79 for clinopyroxenes. This large difference between Mg numbers of orthopyroxenes (OPx) and clinopyroxenes (CPx) suggests a chemical disequilibrium in the initial sample. This difference of Mg numbers of coupled OPx and CPx is a common feature in gabbronorites of the Haymiliyah section, as described by Dahl (1984).

4 EXPERIMENTAL SETUP AND DATA ANALYSIS

Internal friction spectroscopy of rocks has been the object of several torsion experiment studies (e.g. Guéguen *et al.* 1981; Berckhemer *et al.* 1982; Gribb & Cooper 1998; Jackson *et al.* 2000).

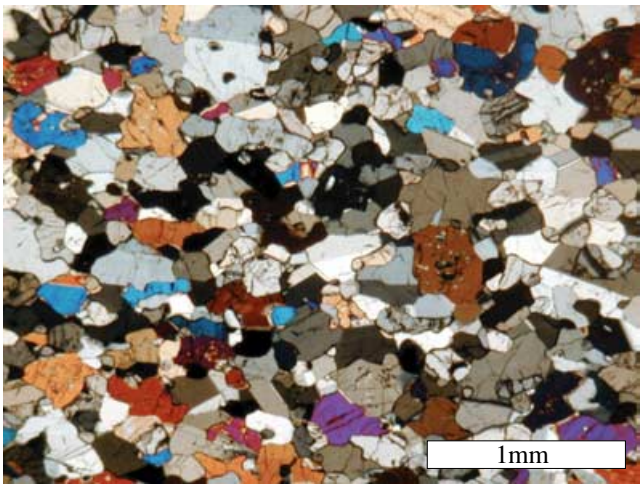

Figure 1. Optical microphotograph of the original gabbronorite sample. The rock displays a mosaic texture with polygonal plagioclase, planar to curviplanar grain boundaries, 120° triple junctions and equigranular grains, which are the expression of a microstructural equilibrium.

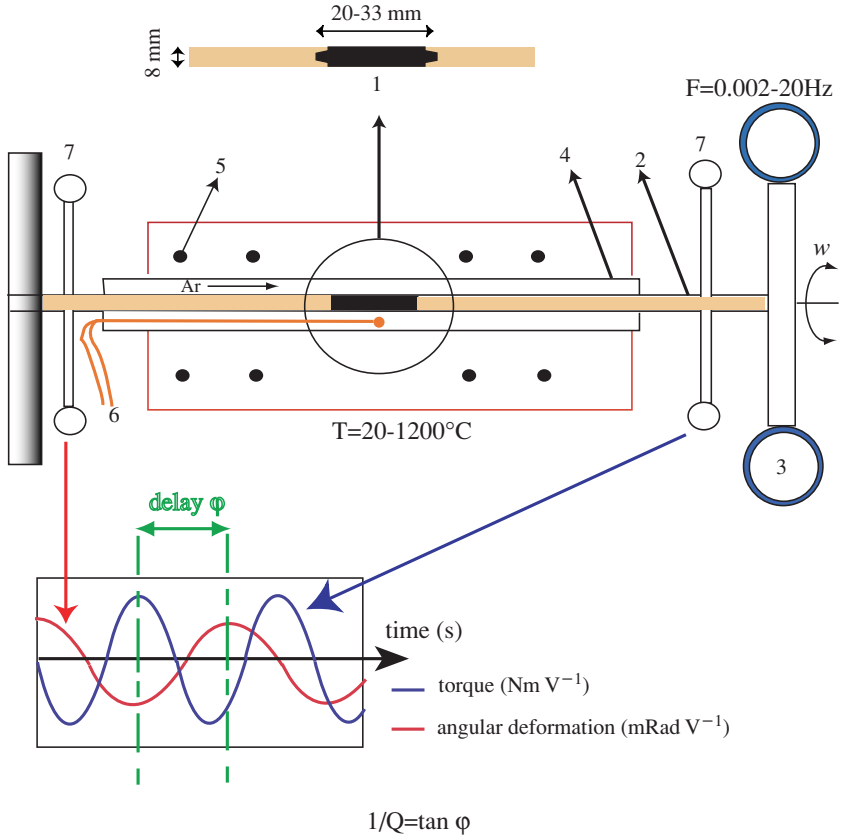

Figure 2. Torsion device. The cylindrical sample (1) is placed between two alumina rods (2). One extremity of this bar is fixed; the torque applied to the other extremity is harmonically generated by a pair of moving electromagnets (3) connected to a synthesizer via a power amplifier. The sample–rod assembly is placed in an alumina pipe (4) in the tubular furnace (5), a thermocouple (6) measures the temperature. The torsional deformation of the sample is measured in two points by two pairs of transducers (7). At each temperature and for various frequencies the phase delay is measured, and Q^{-1} is given by eq. (1).

Our experimental device (Fig. 2) is a forced-oscillation apparatus, designed by H. Berckhemer and E. Aulbach (Berckhemer *et al.* 1982), and improved by Bagdassarov & Dingwell (1993) and James *et al.* (2004). Cylindrical cores (8 mm in diameter, 20–33 mm in length) were drilled out from the rock sample. Five cores (Gab2, Gab4, Gab5, Gab7, Gab8,) are perpendicular to the foliation and one core (Gab3) is parallel to the foliation. At both ends of the cylinders, small conical grips were machined with a diamond tool (Fig. 2). The cylinders are placed in the torsion device after being glued between two alumina rods with the high temperature cement Polytec®. The cylinder is then sintered to the rods during 5 hr at 300°C and at 550°C over 24 hr under the axial load of 8 N, applied by a flat spring (Berckhemer *et al.* 1982). The temperature is maintained at 700°C during 14 hr, before further heating to higher temperatures. One end of the cylinder +2 alumina rod assembly is fixed; the torque is applied to the opposite alumina rod. The mechanical torque is harmonically generated by a pair of moving coil electromagnets connected to a signal function generator via a power amplifier. The cylinder +2 alumina rod assembly is placed in a tube furnace controlled by a Eurotherm controller. A *S*-type thermocouple is used to measure the temperature in the close vicinity of the sample. One pair of capacitor pick-up transducers is used to measure the angular deformation of the alumina rod with respect to the fixed end, and another pair of transducers measures the total angular deformation of the assembly (consisting of the sample and the two alumina rods). For each measurement the data are collected over two periods of the torsional oscillation. Data are sampled at up to 10 kHz, allowing 1000 signal samples per channel to be acquired at the highest frequency of the measurement (20 Hz). At torsional oscillation frequencies of 2 Hz or lower, the number of signal samples per channel is limited to 10 000. The collected signals are automatically fitted to the sinusoids using a Levenberg–Marquardt algorithm, and the phase difference between the applied torque and the angular displacement across the sample are calculated from the phase and amplitude parameters of the fitted curves (James *et al.* 2004). During calibration experiments the shear modulus of the single alumina rod has been measured in the torsion apparatus. Then, the single alumina rod has been cut into two rods. Knowing the lengths between the points where the transducers were fixed and the position of the sample, the diameter, the shear modulus of the alumina rods (which were determined in the independent single rod torsion experiments), and the applied torque $T_{\text{applied}}(\approx 10^{-5}$ N m), the angular deformation in the alumina rods can be calculated and subtracted from the total deformation of the assemblage consisting of the sample and the two alumina (see Figs 3a and b in Bagdassarov & Dingwell 1993). The calibration methods of torque and angular deformation measurements are explained in details elsewhere (Bagdassarov & Dingwell 1993; Bagdassarov 2000). From the angular deformation and the phase delay $\varphi(\omega)$ in the sample, the complex shear modulus and the intrinsic internal friction Q^{-1} are calculated (Bagdassarov & Dingwell 1993). The torque calibration has been done in static conditions by applying small weights of 0.1 g. The test experiments on dummy samples of Al_2O_3 ceramics, having the same shape as a rock sample, showed a negligible effect of sintered mechanical contacts between alumina

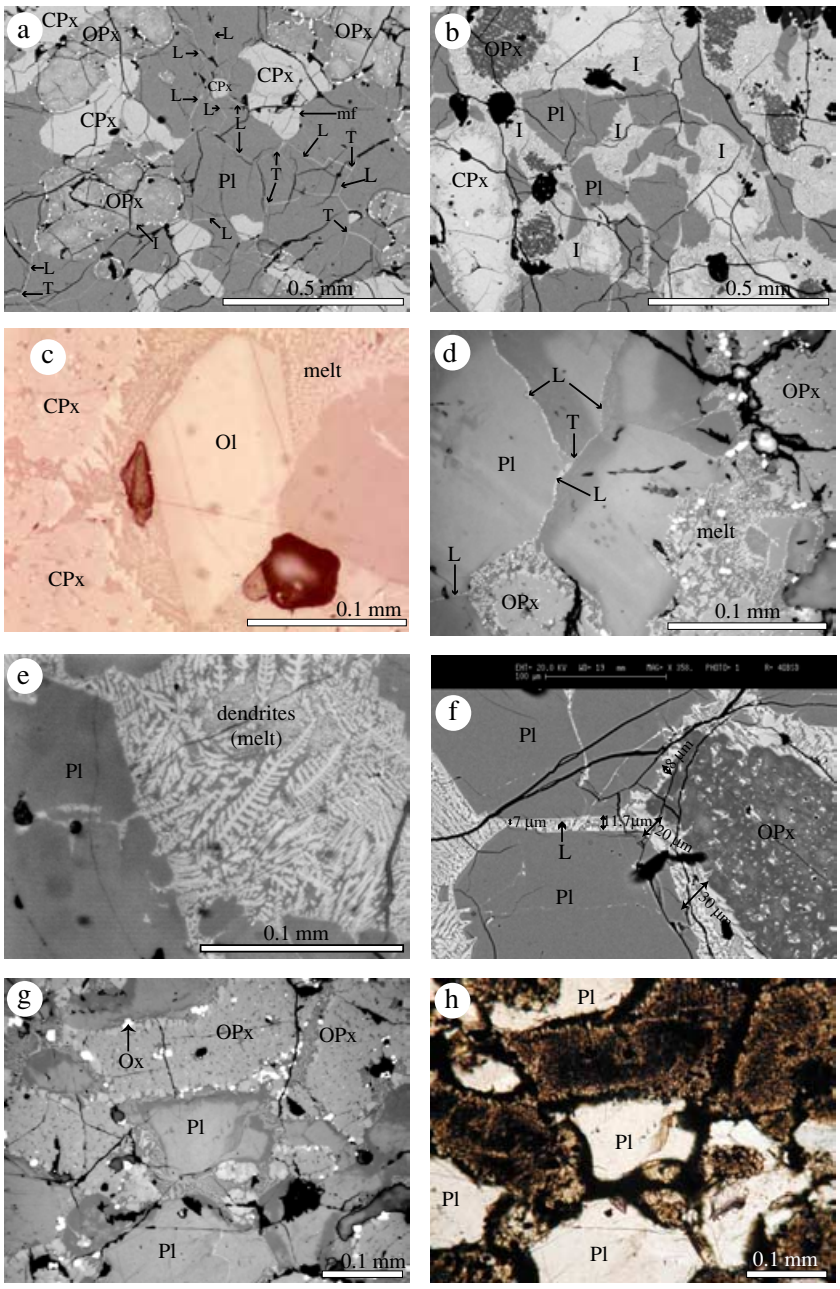

Figure 3. Backscattered SEM microphotographs (a, b) and optical microphotographs (reflected light, c to g; transmitted light, h) of partially molten samples after experiments (Gab2, T_{max}1162°C : g and h, Gab3, T_{max}1168°C : c, f and e, Gab4, T_{max}1154°C : d, Gab6, T_{max}1137°C: a, Gab7, T_{max}1165°C : b). Backscattered SEM images (a and b) were used for image analysis and melt fraction estimates. The long, melt-free cracks are second-generation cracks due to the quick cooling. Images g and h illustrate how oxidation of the phases resulting from melting allows one to identify, on the first order, the melt phase in optical images. The texture is marked by the occurrence of (i) melt at triple junctions (T), (ii) melt films, a few μm thick, between two grain boundaries (L), and melt surrounded by a minimum of four grains (I). Pl = plagioclase, CPx = clinopyroxene, OPx = orthopyroxene, Ox = oxide.

rods and a sample even at temperatures up to 1300°C (Bagdassarov & Dingwell 1993).

The difference in temperature between the sample centre and the sample extremity was measured using the *S*-type thermocouple, which was moved alongside the sample at three different furnace temperatures: 500°C, 1000°C and 1170°C. The temperature difference is less than 5°C at temperatures below 1000°C and *c*. 10° at 1170°C. This may slightly affect the results of Q^{-1} measurements. For the data processing a corrected averaged temperature of the sample measured at the middle part and at the ends has been used. During the experiments the furnace was purged with flowing argon ($5\,cm^3\,s^{-1}$) in order to reduce oxidation of sample surfaces. The fO_2 of the argon flow is from 10^{-4} to 10^{-3} bar. The oxidation or reduction of the grain boundary surfaces may affect the internal friction of the samples. This may be important for samples without melt and when the oxidation–reduction occurs in a large volume of the sample. The sample diameter is 8 mm, and it would take a long time to oxidize or reduce the whole interior of the sample. The destruction of grain boundaries in the sample interior due to the oxidation–reduction processes was not observed from the thin sections after the experiments. The grain boundary oxidation or reduction would produce an effect of a minor importance on the

internal friction in samples with partial melting. Measurements of complex shear modulus and phase shift, between the applied torque and the resulted angle deformation, were done at fixed frequencies (2×10^{-3}–20 Hz) and at increasing temperature steps. This procedure was chosen, rather than decreasing temperature steps, in order to prevent crystallization from the melt phase during measurements and to reduce thermal cracking. Crystallization of minerals could produce an additional relaxation mechanism due to an increasing cohesion on the grain boundaries (e.g. Bagdassarov 2000). The sample was held at constant temperature for at least 2 hr prior to a start of Q^{-1} measurement.

In order to verify the harmonic distortion of measurements, in experiment Gab7 we analysed the sinusoidal torque and angle deformation signals up to 1120°C, by using the fast Fourier transformation. At 1120°C and 5×10^{-3} Hz, the amplitudes of second, third and higher harmonics of the applied sinusoidal torque and of the response signal were lower than 2–3 per cent of the amplitude of the main frequency, showing that the torsion deformation and the sample response was almost linear even in experiments at highest temperatures (James *et al.* 2004).

Several measurements of Q^{-1} (e.g. Kampfmann & Berckhemer 1985; Jackson *et al.* 2002) at low frequency, various temperatures, and different kinds of rocks have shown that a power law could describe the experimental data of Q^{-1},

$$Q^{-1}(\omega, T) = A \cdot [\omega^{-1} \cdot \exp(-Ea/RT)]^{\alpha}, \quad (3)$$

where ω is the frequency of oscillations, T is the absolute temperature, E_a is the activation energy, α is the empirical exponent, A is a pre-exponential constant.

To estimate the influence of temperature on dissipation, the eq. (3) has been transformed into a logarithmic form, and the measured Q^{-1} for each experiment were fitted to a multilinear regression. 3 preliminary experiments of Bagdassarov (2000) with Oman gabbro samples were also included in the data processing. Some of the measurements were done at decreasing temperature steps, and thus Q^{-1} was probably underestimated as the melt phase was partially crystallizing during rapid and decreasing temperature steps. Therefore, only the data corresponding to increasing temperature steps or to the maximum temperatures has been considered in the data analysis.

In order to examine the grain size effect on Q^{-1}, eq. (4) was used, where a grain size was introduced as a power law dependence (Jackson *et al.* 2002).

$$Q^{-1}(\omega, T, d) = A \cdot d^{-m}[\omega^{-1} \cdot \exp(-Ea/RT)]^{\alpha}, \quad (4)$$

where d is the grain size parameter and m, α are the empirical exponents.

In this study we use both a linear regression, as suggested by Jackson *et al.* (2000, 2002), and a multilinear regression fitting of Q^{-1} variations with temperature and frequency.

5 RESULTS

5.1 Microstructures

Experiments were stopped at differing maximum temperatures in order to relate the Q^{-1} variations to the melt fractions and/or melt geometry observed in the samples. After (slow) cooling (at a rate of $\sim$16°C min^{-1}) of samples, the quenched phases resulting from melting, that is, glass and crystals, were studied by optical and electronic microscopy (Fig. 3). Many intergranular cracks are present after experiments (Fig. 3), but they were not filled by melt. We assume that these are late cooling features, and had no effect on the measured phase delay with increasing temperature. They likely result from the thermal contraction of the sample during cooling at the end of experiments.

The partial melt topology changes with temperature. The classification of Cmíral *et al.* (1998) was used in order to discuss of the melt distribution in our samples. At 1123°C and 1137°C the melt phase is present (Fig. 3)

(i) as thin $\sim$1 μm thick layers (L) between plagioclase grains,
(ii) in irregularly (I) shaped pockets around the enstatites and
(iii) at triple junctions (T).

Although melt-free grain boundaries are observed between clinopyroxene–plagioclase pairs, and clinopyroxene–orthopyroxene pairs (Fig. 3a), we cannot exclude the presence of thin films or impurity *c*. 1 nm thick in the aggregate observed by others using TEM (e.g. Cmíral *et al.* 1998). At T_{max} = 1123°C and 1137°C (Fig. 3a), enstatite grains are surrounded by oxides (magnetite) and a melt phase. Enstatite melting is incongruent at room pressure and results in the crystallization of idiomorphic olivine, which is observed in samples Gab3 (T_{max} = 1168°C; Fig. 3c), and Gab7 (T_{max} = 1165°C). A melting of anorthite, diopside and enstatite is predicted by liquidus phase relationships in the forsterite–diopside–anorthite–silica system (e.g. Cox *et al.* 1979). However, no melt phase is observed at clinopyroxene boundaries. At T_{max} = 1137°C (Fig. 3a), melt was preferentially located at plagioclase–plagioclase and plagioclase–enstatite boundaries. Most grain boundaries are wetted at and above 1165°C (Figs 3b–h). At 1165°C the width of melt pockets is $\sim$10–15 μm. The relict grains are xenomorphs and can be distinguished from newly crystallized automorphs grains. Enstatites are more progressively melted than other crystals (Figs 3f–h); about half of the enstatites are molten at 1165°C. The melt fraction (at grain boundaries, and in intergranular pockets) was estimated by image analysis, from series of backscattered electron images in each sample. It was then possible to plot the melt fraction as a function of temperature (Fig. 4). The distribution of melt is heterogeneous. In the thin section of Gab7 (T_{max} = 1165°C), the melt fraction is around 4 per cent at the sample extremities and up to 20 per cent at the centre, with an average value of 10 per cent. The distribution of melt is consistent with temperature variations along the sample, rather than reflecting heterogeneity of composition. In the melt fraction estimate we have not considered the crystallization of oxides during cooling. Thus, we may underestimate the melt fraction present during the experiments. However, the majority of oxides observed at the end of the experiments likely crystallized during the partial melting, using FeO from pyroxenes.

At 1123°C and 1137°C, the average crack aspect ratio has been estimated (ratio of a thickness of a disk-shaped melt pocket to its diameter) to be in the order of 10^{-3}. At 1165°C the average crack aspect ratio is about 10^{-2}. This increasing aspect ratio with temperature is due to the increasing width of the melt pockets between 1137°C and 1165°C. At high temperatures, melt is mostly present in films and is well connected; the solid crystalline framework is progressively disaggregated by melt.

Whatever the foliation orientation was with respect to the applied torque, melt is preferentially aligned in the foliation (Fig. 5). The melt phase is indirectly visualized by the oxidation (Figs 3g–h and 5) of the phases, which crystallized from the melt. The preferred orientation of plagioclase (010) crystallographic planes defines the foliation; the preferred orientation of plagioclase [100] crystallographic axes and orthopyroxene [001] crystallographic axes define the lineation (Fig. 6). The measured crystallographic preferred

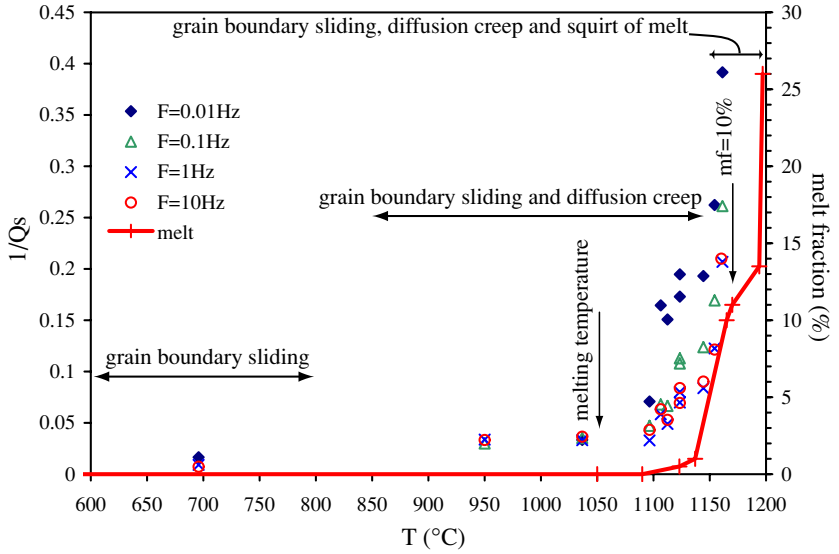

Figure 4. Melt fraction and Q^{-1} variation as a function of the maximum temperature for samples perpendicular to (X,Y). The melt fraction estimates have been obtained by image analysis of back-scattered electron microphotographs (Figs 3a and b). Melt fractions at 1170, 1194 and 1197°C are deduced from the previously published preliminary experiments (Bagdassarov 2000). The vertical arrow at 1050°C indicates the onset of melting and the vertical arrow at 1165°C indicates a melt fraction (mf) ∼10 Vol. %. Various regimes in the attenuation behaviour are indicated by the 3 horizontal double arrows (modified from Pezzotti 2003). Below 800°C attenuation is due to grain boundary sliding. Between 850°C and 1150°C attenuation is attributable to grain boundary sliding and diffusion creep. At temperature higher than 1150°C attenuation is caused by grain boundary sliding, diffusion creep and the melt squirt flow.

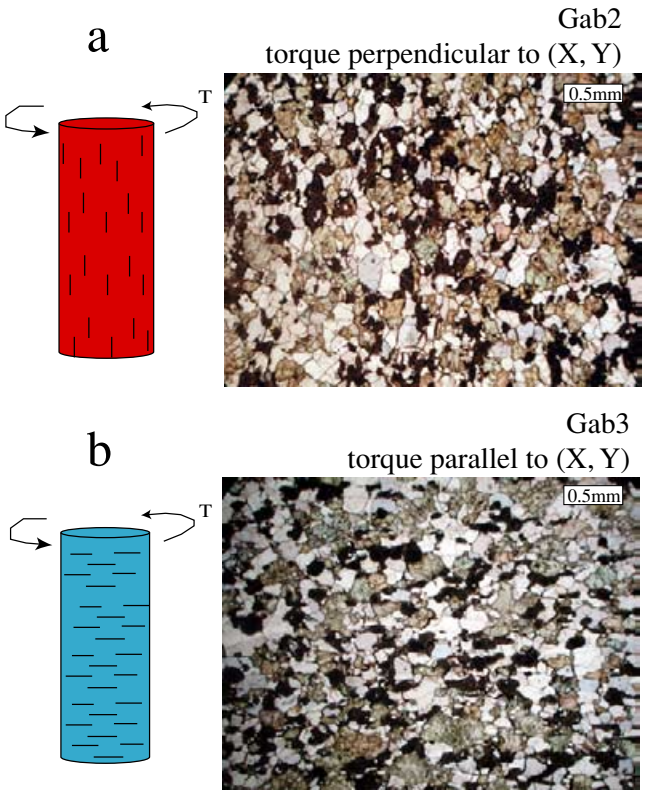

Figure 5. Optical microphotographs (transmitted light) showing the anisotropy of the melt phase distribution, as estimated from oxidation of the phases resulting from partial melting. (a) Sample Gab2, torque was applied perpendicular to foliation. (b) Sample Gab3, torque was applied parallel to foliation. In both cases the melt phase was preferentially aligned with the foliation.

orientations of plagioclase are similar before and after experiments; no macroscopic plastic deformation has occurred during experiments.

5.2 Melt viscosity

The melt viscosity is an important parameter of viscoelasticity of partially molten rocks because both the melt viscosity and the melt distribution control the relaxation times of the viscous shear, and the melt squirt flow between crystal grains (O'Connell & Budiansky 1977). A change in the melt viscosity of one order of magnitude could result in a change in the location of the relaxation peak of the active attenuation mechanism (e.g. O'Connell & Budiansky 1977). Schmeling (1985, Fig. 6) computed the characteristic frequency of two melt related relaxation mechanisms: viscous shear relaxation, and melt squirt relaxation in tubes and films as a function of melt viscosity and aspect ratio. The main conclusions of his study can be summarized as follows:

(i) Viscous shear relaxation is important in the seismic frequency range for an aspect ratio lower than 10^{-4} and for viscosity higher than 10 Pa s.

(ii) The characteristic frequency of the melt squirt relaxation in tubes is in the seismic frequency range (0.01–100 Hz) for aspect ratios between 10^{-2}–10^{-3} and viscosity in the range 10^{2}–10^{4} Pa s.

(iii) The characteristic frequency of the melt squirt relaxation in films is in the seismic frequency range (0.01–100 Hz) for aspect ratios between 10^{-2}–10^{-3} and viscosity higher than 10 Pa s.

The melt viscosity can be estimated from chemical analyses of the phases resulting from melting. Chemical compounds were analysed with a Cameca SX100 electronic microprobe. Analysis of glasses and dendrites (60 per cent surface of the inferred melt phase after cooling) in a thin section of sample Gab3 (T_{max} = 1168°C)

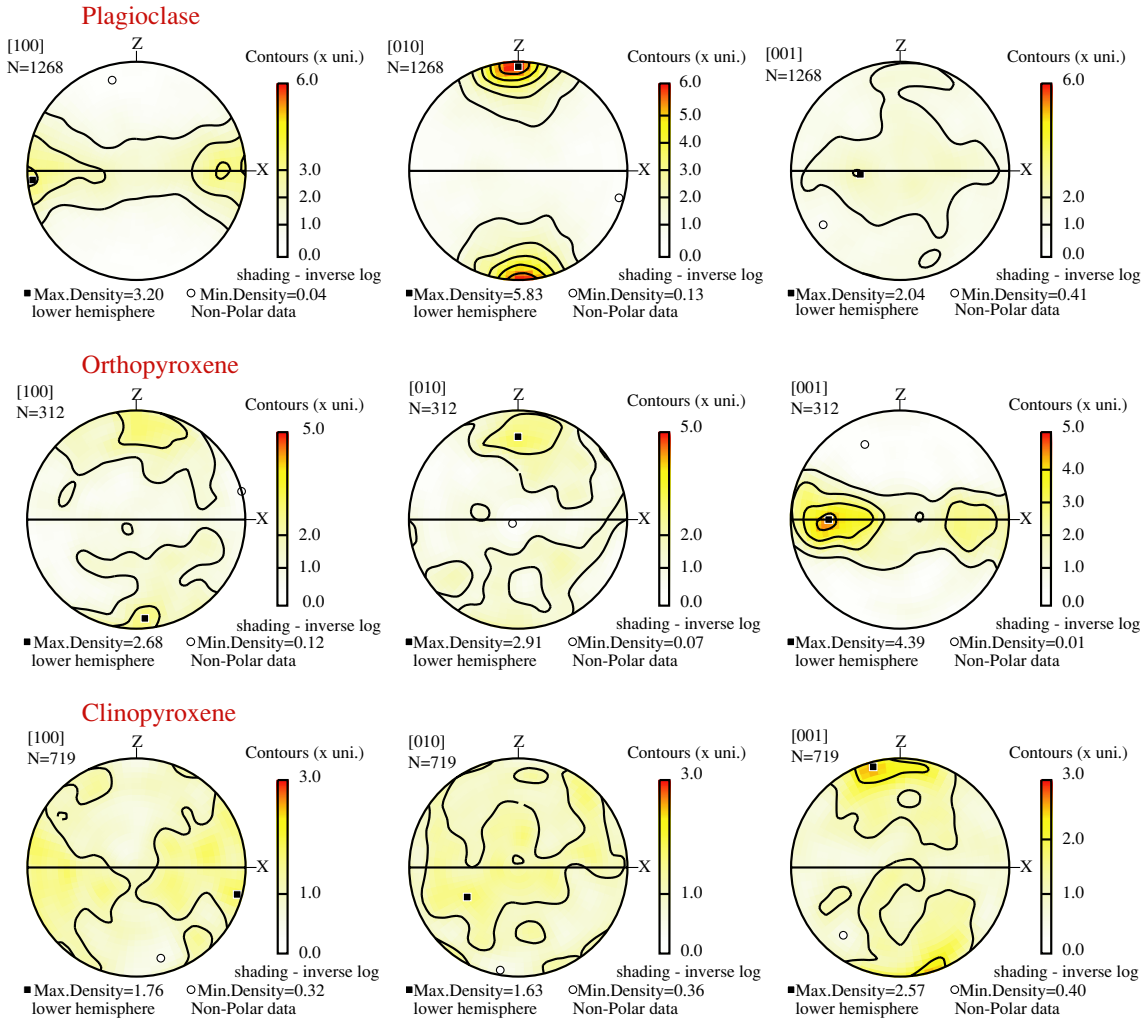

Figure 6. Crystallographic preferred orientations of plagioclase, clinopyroxene and orthopyroxene measured in the gabbronorite before torsion experiments. [100], [010] and [001] pole figures plotted in lower hemisphere with the foliation defined by the horizontal solid line. *N* is the number of measurement.

Table 1. Chemical compositions (in weight of oxides, per cent) of sample Gab3 ($T_{max} = 1168°C$) analysed on Cameca SX100 electronic microprobe (beam parameters 20 kV and 10 nA). Bytownite (Btw), diopside (Di) and enstatite (En) are the initial phases. Magnetite (Mgt), forsterite (Fo), glasses and dendrites are phases resulting from partial melting. The high Al_2O_3 contents in glasses and dendrites are related to plagioclase (bytownite) melting. SiO_2, FeO, MgO and CaO contents result from the melting of enstatite and diopside.

	Btw	Di	En	Mgt	Fo	Glass compositions				Dendrite compositions			
	Pl1	Cp1	Op1	Ox1	Ol1	V1	V2	V3	V4	D1	D2	D3	D4
SiO_2	45.79	52.16	54.95	0.27	41.39	54.44	54.77	55.23	54.43	48.55	48.22	48.69	46.53
Al_2O_3	34.38	2.08	1.28	6.89	0.05	17.33	17.98	17.70	17.61	11.26	10.37	10.12	8.81
FeO	0.59	7.67	9.71	76.44	6.56	8.92	8.94	8.95	7.88	10.38	10.46	9.74	9.60
CaO	17.70	21.27	1.76	0.28	0.26	9.76	9.80	10.34	10.45	15.54	15.74	14.13	19.16
MgO	0.06	14.93	32.39	7.74	50.87	4.17	3.63	4.92	3.70	12.70	13.82	16.59	14.39
Na_2O	1.22	0.25	0.02	0	0.01	1.32	1.21	2.24	2.30	0.38	0.35	0.30	0.22
TiO_2	0.01	0.32	0.13	0.25	0	0.23	0.27	0.24	0.22	0.23	0.19	0.18	0.23
K_2O	0.01	0	0	0	0	0.21	0.18	0.09	0.09	0.04	0.03	0.02	0
MnO	0.01	0.20	0.33	0.35	0.24	0.17	0.15	0.16	0.11	0.28	0.25	0.25	0.17
NiO	0	0.02	0.05	0.22	0.21	0	0	0	0	0.02	0.03	0.03	0.01
Cr_2O_3	0	0.08	0.01	0.29	0.02	0.01	0.02	0	0	0.03	0.05	0.01	0.03
Total	99.77	98.99	100.62	92.72	99.60	96.56	96.94	99.87	96.78	99.41	99.50	100.06	99.15

are summarized in Table 1. The melt appears to be chemically homogeneous in the sample. Melt located at plagioclase–plagioclase boundaries, at plagioclase–orthopyroxene boundaries, and at plagioclase–clinopyroxene boundaries have roughly the same chemical composition. Measurements of the viscosity from the glass transition to superliquidus temperatures were conducted in a creep apparatus and in a rotational Couette viscometer (Fontaine & Neuville, in preparation, 2005). The results are consistent with the

viscosity calculations according to models of Shaw (1972) and Bottinga & Weill (1972), with a value of $\eta = 310$ Pa s at 1168°C for a liquid with a chemical composition equivalent to the sum of chemical compounds in glasses and dendrites of Gab3.

5.3 Attenuation

In all experiments, at a given temperature, Q^{-1} varies strongly with frequency (Fig. 7). High attenuation (∼0.1) is reached even without any melting. Below the melting temperature (∼1050°C), the frequency dependence of attenuation is weak in all experiments, with an average slope of −0.15 at low frequencies (≤0.5 Hz), and −0.06 at higher frequencies. Above the melting temperature, the dissipation increases significantly, and a stronger frequency dependence is observed, with an average slope of −0.22 at low frequencies, and 0.02 at higher frequencies. At low frequencies (<0.5 Hz) and temperature above 1050°C, the stronger frequency dependence is probably related to the extended viscoelastic behaviour of the rock (generalized Maxwell-body behaviour). Between 1057°C and 1085°C, the attenuation increase is stronger, compared to lower temperature steps. The temperature dependence of attenuation is best illustrated by comparing Q^{-1} measured at four different frequencies (Fig. 8). Above 1050°C, the slope of the curve is steeper, with an attenuation increase of approximately one order of magnitude for a temperature interval of 100°C. In one experiment (Gab5 at 1144°C), Q^{-1} decreased by 0.03 after 24 hr at the same temperature. This observation may be due to the topological equilibration of the melt phase, which is more stable after 1 day at a given temperature and implies that the melt geometry has been changed. The melt flow in a sample under torsion deformation likely became less efficient because the melt has already migrated toward more favourably oriented geometry. In this study, the possible time dependence of the microstructure

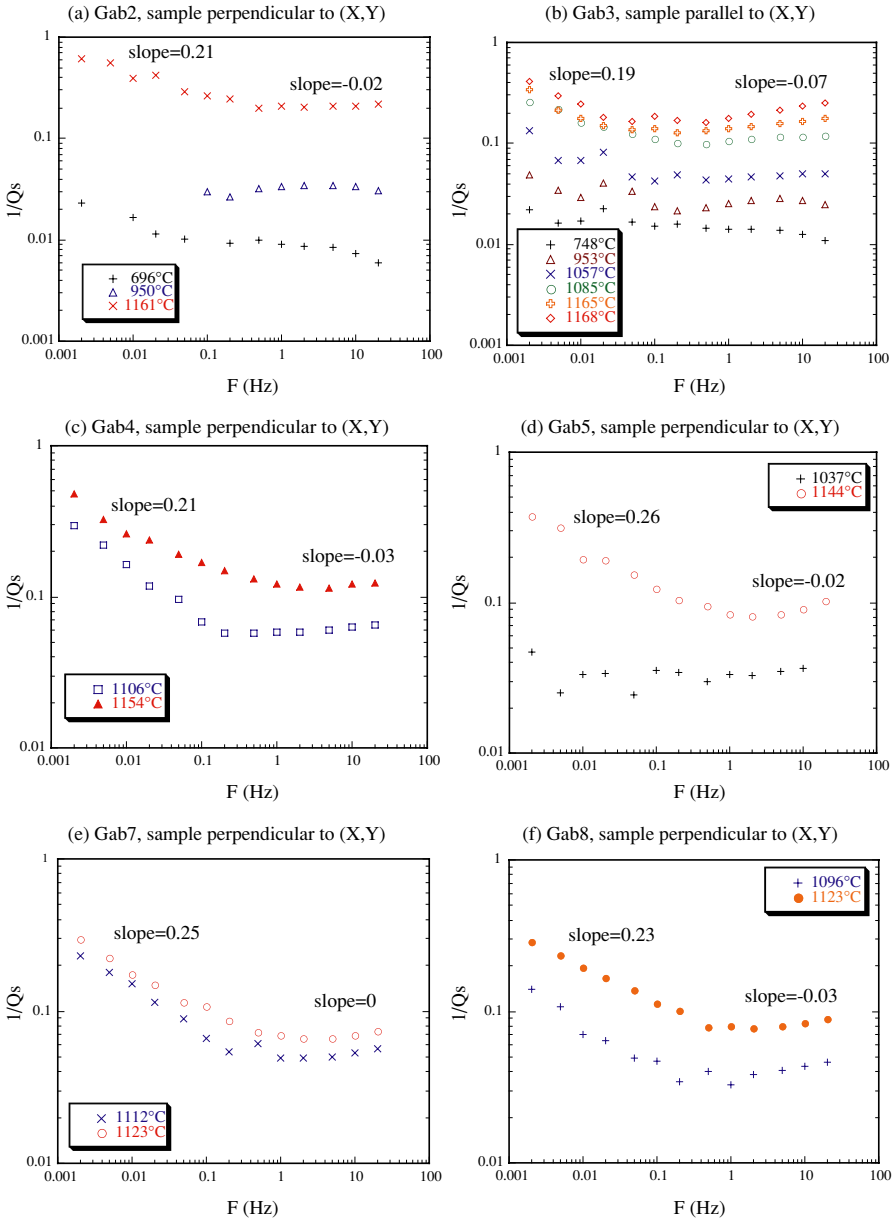

Figure 7. Q^{-1} as a function of temperature and frequency. In all experiments, and at constant temperature, Q^{-1} changes with frequency. The slopes (angular frequency dependence) are indicated on each curve; slopes are calculated for two frequency domains (0.002–0.5 Hz and 0.5–20 Hz). At low frequency (<0.5 Hz) and for temperatures above 1050°C the stronger frequency dependence results from the viscoelastic behaviour of the samples (see text for further discussion).

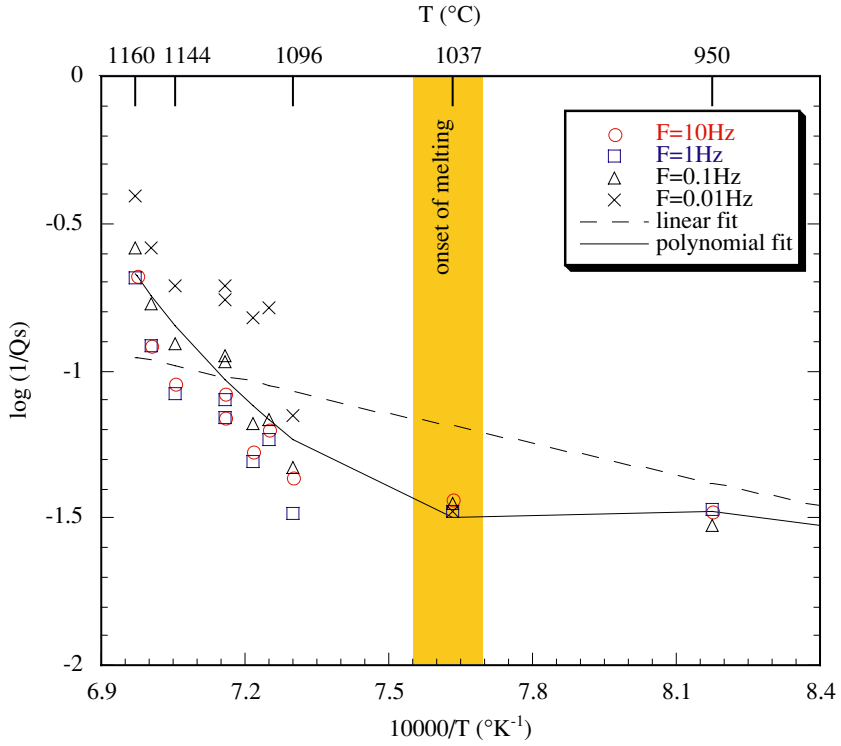

Figure 8. Measurements of Q^{-1} as a function of the reciprocal absolute temperature and at four distinct frequencies: 0.01, 0.1, 1 and 10 Hz in samples perpendicular to (X, Y). Note that above the melting temperature the increase of Q^{-1} is higher at the lowest frequency. The linear fit equation used in this plot is $\log Q^{-1} = 3541/T + 1.5156$, with a correlation coefficient of 0.79. A better fit is obtained by the polynomial fit: $\log Q^{-1} = -0.345536z^3 + 8.930143z^2 - 76.354754z + 214.692715$, where $z = 10000/T$ and with a correlation coefficient of 0.91.

during the experiment at a constant temperature has not been explored further.

At high temperature and low frequencies Q^{-1} increases exponentially as the temperature increases towards the melting point. This behaviour is called 'high temperature background' (HTB) absorption in the literature (e.g. Nowick & Berry 1972; Jackson 2000). We used eq. (3) to compute Q^{-1} for the HTB. The correlation coefficient between measured Q^{-1} and calculated Q^{-1} for the HTB is 0.84 on average. Above 1050°C, the measured Q^{-1} is higher than the calculated Q^{-1} for HTB. Consequently, an additional mechanism must be effective to explain the measured Q^{-1}. We assume it is related to the presence of melt and probably to melt squirt flow above 1050°C.

Testing the correlation of Q^{-1} with temperature, using a linear regression as Jackson *et al.* (2002; Fig. 9), we find that $Q^{-1} \sim A{\cdot}X^{-0.08}$, where $X = \omega^{-1} \exp(-E_a/RT)$, for an activation energy of 873 ± 13 kJ mol^{-1}, $A = 34.72\,\mathrm{s}^{-\alpha}\,\mu\mathrm{m}^{-\alpha}$, and a correlation coefficient of 0.86. This value of the activation energy corresponds to the minimum standard deviation between the measurements of Q^{-1} and the linear regression fit. In Fig. 9, our measurements of internal friction are compared with measurements in the Anzola gabbro from Kampfmann & Berckhemer (1985) in the frequency range 0.003–30 Hz, at temperature from 775°C to 1000°C, with a grain size of 0.25 mm and an activation energy of $E_a \sim 730$ kJ mol^{-1}. All measurements show an increase of attenuation with an increase of X, a characteristic of the HTB. Our measurements and those of Kampfmann & Berckhemer (1985) give results of the same order of magnitude. However, the trend of near constant Q^{-1} at small values of X is not observed in the study of Kampfmann & Berckhemer (1985). None of the experiments displays a perfect linear behaviour of $\log Q^{-1} \propto \log X$. We find a rather high value of E_a from our experiments, which explains why our high Q^{-1} results were obtained with lower value of X than the other study. The empirical exponent α (i.e. the slope of $\log Q^{-1} = -\alpha \log X + \log A$) is 0.19 in Kampfmann & Berckhemer (1985), and 0.08 in our study. The lower dependence of $\log Q^{-1} \propto \log X$ could result from the presence of higher melt fractions in this study (up to 10 per cent).

Jackson *et al.* (2002) experimentally demonstrated that the seismic wave attenuation is grain size sensitive: Q^{-1} is greater for fine grain specimens than for large grain specimens at a constant temperature and period. Grain size dependence is also illustrated in the general tendency for the parameter A (eq. 3) to decrease with increasing average grain size. Jackson *et al.* (2002) found a better fit to their experimental results by introducing a grain-size parameter to the power law approximation of Q^{-1} (eq. 4). We have tested this fitting option in both our multilinear regression calculation and the linear regression, but our results do not demonstrate a better fit of Q^{-1} when a grain-size parameter is introduces in eq. (3). We have compared the results of Kampfmann & Berckhemer (1985) obtained for three different grain sizes (0.25, 0.5 and 1 mm) at 0.03 Hz and our result at 0.01 Hz but we find no clear correlation with the grain size (Fig. 10). This absence of correlation between $Q^{-1}(\omega)$ and the grain size d is consistent with a nearly frequency independent internal friction observed in torsion experiments at frequencies higher than 0.5 Hz. In this study, it may also be due to the measurement noise, higher in our measurements than in measurements of Jackson *et al.* (2002). The average standard deviation of $Q^{-1}(\omega)$ for all experiments is lower than 0.03 below 1 Hz, and lower than 0.006 above 1 Hz. Kampfmann & Berckhemer (1985) pointed out that 'no clear dependence of Q^{-1} on grain size can be stated' from their experiments. With the present study, we cannot clearly establish a relationship between Q^{-1} and the grain size d.

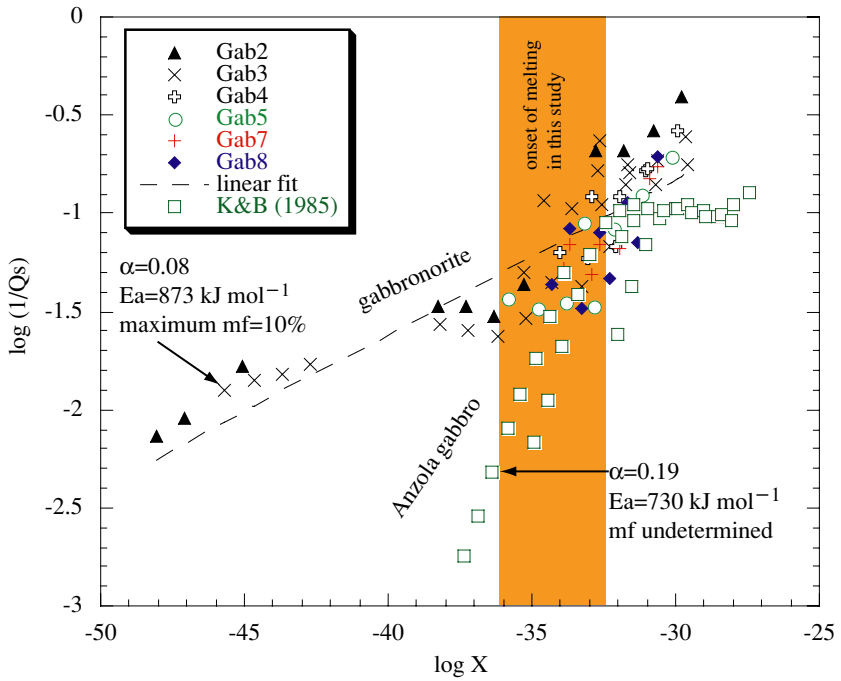

Figure 9. Comparison of Q^{-1} data at four different frequencies (0.01, 0.1, 1, and 10 Hz), with a model where Q^{-1} is approximated by a power-law (eq. 3). The straight line corresponds to a fit on our data: with a continuous variation of a slope in the dependence $\log Q^{-1} \propto \log X$, where $X \sim \omega^{-1} \exp(-E_a/RT)$, our model is $Q^{-1} \sim A \cdot X^{-0.08}$, for an activation energy of 873 kJ mol^{-1}, $A = 34.72\,\mathrm{s}^{-\alpha}\ \mu\mathrm{m}^{-\alpha}$. Measurements of Kampfmann & Berckhemer (1985) for an Anzola gabbro (grain size ~250 μm) are also plotted for comparison with our data (grain size ~250 μm). mf is the melt fraction estimation, E_a is the activation energy, and α is the empirical exponent (i.e. the slope). Note the lowest value of α found for our experiments and the highest value of E_a. K & B is the abbreviation of Kampfmann & Berckhemer (1985).

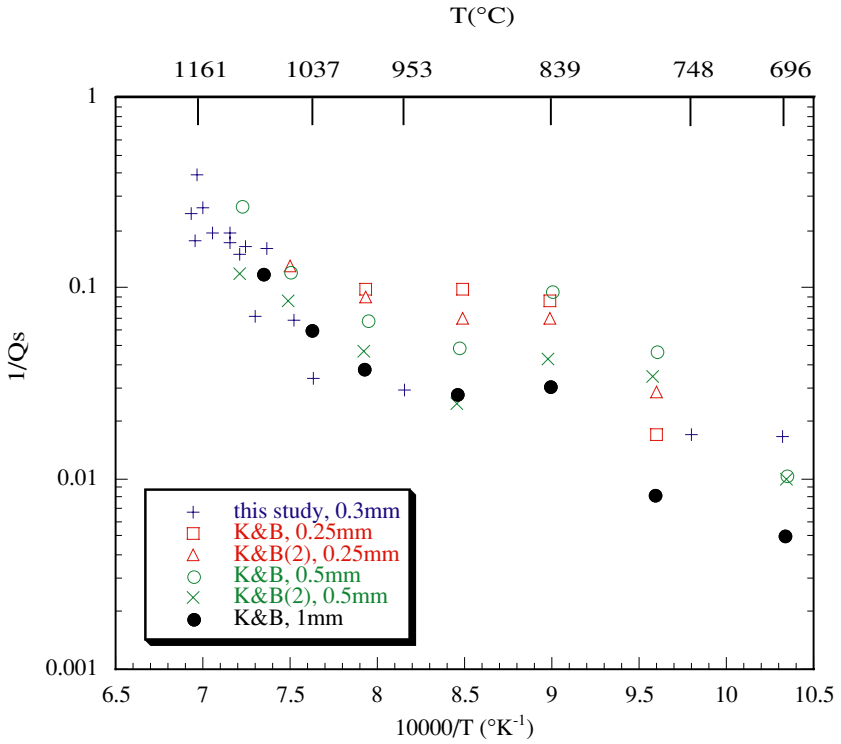

Figure 10. Comparison of measured Q^{-1} as a function of temperature in this study (0.01 Hz, grain size ~0.25 mm), and in Kampfmann & Berckhemer (1985), at 0.03 Hz and with 3 different grain sizes (0.25 mm, 0.5 mm, 1 mm). A weak correlation between $Q^{-1}(\omega)$ and the grain size d is consistent with a nearly frequency independent internal friction observed in torsion experiments.

6 DISCUSSION

6.1 Comparison with previous studies

The experiments of Kampfmann & Berckhemer (1985) were done using a hornblende-gabbro from Anzola (Ivrea Zone, Western Alps, Italy). The measurements were realized at temperatures $\leq$1100°C. The presence of a small amount of melt was inferred from the results at 1000°C, but it was not measured directly from samples. Q^{-1} values were either of the same order of magnitude as our results, or up to one order of magnitude higher than ours at 10 Hz. Kampfmann & Berckhemer (1985) found a weak dependence of Q^{-1} to frequency at the highest temperatures ($\geq$1000°C). At low temperatures (700–950°C) they observed a flat absorption peak superimposed on the HTB, and they noted the shift of this peak from high to low frequencies with a decreasing temperature (fig.12 in Kampfmann & Berckhemer 1985). Bagdassarov (2000) has observed below the softening temperature a general dependence of $Q^{-1} \sim \omega^{-0.17\pm0.01}$ at low frequencies (<0.5 Hz). Above the softening temperature, the empirical exponent α was higher than 0.35 at low frequencies (<0.5 Hz).

In our experiments we do observe a small part of the low-frequency shoulder of the attenuation peak, which shifts from high to low frequencies with a decreasing temperature (Fig. 7) as it was observed by Kampfmann & Berckhemer (1985). The sign of the slope ($-\alpha = \Delta\log(1/Q_S)/\Delta\log\omega$) in the plot of $1/Q_S$ versus frequency (Fig. 7) changes at higher frequencies with increasing temperature. The frequency shift seems to have a smaller effect than the temperature shift.

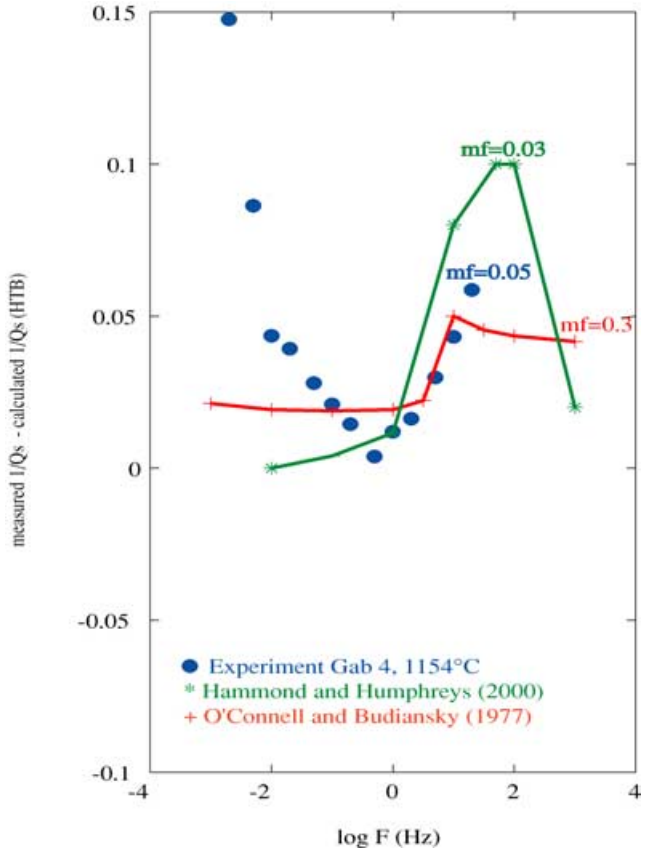

Figure 11. The difference between measured Q^{-1} and calculated, temperature-related Q^{-1} (HTB, see text for further discussion) is represented by circle as a function of frequency and is compared with 2 models of melt squirt flow (O'Connell & Budiansky 1977; Hammond & Humphreys 2000) for various melt fractions (mf). Except for the low frequencies (<0.5 Hz), where measurement errors are high (up to 10 per cent at 0.002 Hz), the difference between the measured Q^{-1} and the HTB-related calculated Q^{-1} shows the same frequency dependence as internal friction calculated for squirt flow.

The activation energy estimated from the linear regression in this study is higher that the value of the activation energy estimated for the Anzola gabbro (Kampfmann & Berckhemer 1985). In the presence of impurities, larger activation energy might be expected (Jackson 2000). In this study, the estimated activation energy is also higher than the experimentally estimated E_a in a fine-grained anorthite for the diffusion creep. Dimanov *et al.* (1998) obtained an activation of energy of 365 kJ mol^{-1} for the partially molten plagioclase aggregates in the diffusion creep regime. Dimanov *et al.* (1999) found $E_a \sim$ 585 kJ mol^{-1}, Rybacki & Dresen (2000) 467 kJ mol^{-1}, Montardi (1987) 715–750 kJ mol^{-1}, and Wang *et al.* (1996) 420 kJ mol^{-1} in a fine-grained polycrystalline anorthite for the diffusion creep. The higher activation energy herein could be due to the effect of the temperature dependent melt fraction (e.g. Tan *et al.* 2001). The creep activation energy cannot be precisely measured, because the melt volume fraction increases with increasing time of the sample deformation (e.g. Ji 1987).

6.2 Textures

At 1165°C, grain boundaries are irregular and the melt phase is mostly connected in the sample. The melt phase starts to be connected when the melt fraction is comprised between 1 and 10 per cent. We cannot determine this connection threshold more accurately because none of the torsion experiments were terminated in the temperature range 1140–1160°C. However, this critical melt fraction could be small, in the range 1–2 per cent, thus explaining (1) the significant increase of Q^{-1} above 1100°C at 0.01 Hz (Fig. 4), and (2) the chemically nearly homogeneous composition of the molten phase at 1168°C (Table 1). At this temperature the texture of the molten rock is unlikely to be at the microstructural equilibrium because all the grains boundaries are wet. Microstructurally equilibrated partially molten rocks are not expected to present fully wetted grain boundaries (e.g. Wark *et al.* 2003). Texturally equilibrated partially molten rocks have similar mean grain curvature, which results in constant grain boundary contact between phases (e.g. Bulau *et al.* 1979). The topology of melt is probably not at a perfect steady state in this study because

(1) we observed at 1137°C fully wetted grain boundaries between two grains,

(2) attenuation decreases after one day at a constant temperature (1144°C) and

(3) there is a variation in melt content along the length of the specimen due to finite temperature gradients. At temperature $\leq$1137°C the texture of our partially molten rock is close to microstructural equilibrium because not all grain boundaries are wet and the grain boundaries of plagioclase and clinopyroxene are still curviplanar. At temperature $\geq$1165°C the sample structure is in disequilibrium. Although, textures are close to microstructural equilibrium below 1137°C and there are not above 1165°C, Q^{-1} values obtained at 1085°C, 1165°C and 1168°C show similar frequency dependence (Fig. 7b), we propose that the interconnection of small amount of melt just above the solidus temperature may explain this observation. Sato & Ida (1984) have also observed that the electrical impedance

of partially molten gabbro show very similar frequency dependence above partial melting even for very small amount of melt.

Longhi & Jurewicz (1995) observed melt pockets ($\leq 10\,\mu$m) and melt-free grain boundaries after the melting of a gabbroic anorthosite. Sato & Ida (1984) described in their partially molten ferro–gabbro of Horoman (Hokkaido, Japan) at temperature between 1127°C and 1138°C the occurrence of melt pockets with an average thickness of 50–80 μm and thin melt layers between several grain boundaries. At 1200°C a connected melt phase was observed in the study of Sato & Ida (1984).

The observed melt distribution in our samples is preferentially aligned with the foliation, suggesting that it is controlled by the preferred orientation of plagioclase and pyroxene crystals.

6.3 Mechanisms of attenuation

In partially molten rocks and in the absence of plastic deformation, a major effect is the increase of Q^{-1} with temperature (e.g. Kampfmann & Berckhemer 1985). The HTB was observed in polycrystalline solids (e.g. Kampfmann & Berckhemer 1985) and in single crystals (e.g. Guéguen *et al.* 1989). It is not possible to determine precisely in this study the physical relaxation process responsible for this behaviour.

Above the melting temperature (∼1050°C) the dissipation increases with decreasing frequency in the low-frequency range (Figs 4, 7 and 8). In the high-frequency range, attenuation is almost constant. What are the mechanisms responsible for that behaviour? Numerical models of Q^{-1} relating the internal friction to the presence of the melt phase showed that the melt squirt flow is likely to be the efficient mechanism of the elastic wave attenuation in the seismic frequency range for melt viscosities between 10^2 and 10^4 Pa s and for crack aspect ratio in the range $<10^{-2}$–10^{-3} (Schmeling 1985). The melt squirt flow (Mavko & Nur 1975) may be described as a melt flow from a crack with a high fluid pressure to an adjacent crack with a lower fluid pressure caused by the elastic wave propagation. The characteristic frequency ω of the attenuation maximum for a fluid flow or squirt, corresponding to the transition from saturated isolated to saturated isobaric behaviour, is (e.g. O'Connell & Budiansky 1977)

$$\omega_{\text{squirt}} \approx \frac{K}{\eta}\left(\frac{c}{a}\right)^3, \tag{5}$$

where c/a is the crack aspect ratio (ratio of a thickness c of a disk-shaped crack to its diameter (a), K is the bulk modulus and η is the fluid viscosity. For a partially molten gabbro and a basaltic melt composition, having c/a in the range of 0.01–0.1 and $\eta \sim 10^2$ Pa s, Mavko *et al.* (1998) proposed that the characteristic frequency ω_{squirt} ranges from 50 to 6000 Hz. As described by eq. (5) the characteristic frequency depends on the crack aspect ratio and the shear viscosity of the melt. Assuming a bulk modulus of 50–90 GPa deduced from the measurements at room temperature of *P*- and *S*-wave velocities in gabbronorites (Gebrande *et al.* 1982; Dortman 1976), and extrapolated to high temperatures (Mainprice 1997), and using the shear melt viscosity 310 Pa s (see above), we obtain for the critical frequency peak a value ranging from 0.15 to 300 Hz for a crack aspect ratio between 10^{-3} and 10^{-2}. During the experiments, the crack aspect ratio could change with melt content, and the liquid viscosity could vary with temperature. As there is no direct control during the measurements on both the crack aspect ratios, and on the temperature dependence of viscosity, it is not certain that the melt squirt flow is the melt related attenuation mechanism responsible for the increase of Q^{-1} above the melting temperature.

In all experiments, the difference between the measured $Q^{-1}$and the calculated temperature-related (HTB) Q^{-1} (Fig. 11) is of the same order of magnitude as the values of Q^{-1} due to the melt squirt flow in previously published models (O'Connell & Budiansky 1977; Schmeling 1985; Hammond & Humphreys 2000). This difference is also shown in Fig. 11, as a function of frequency at 1154°C and compared with the melt squirt flow models suggested by O'Connell & Budiansky (1977) and Hammond & Humphreys (2000) for various melt fractions. Except for the lowest frequencies (<0.5 Hz), where the measurement error is high (up to 10 per cent at 0.002 Hz), the difference between the measured Q^{-1} and the calculated HTB-related Q^{-1} shows the same frequency dependence as the Q^{-1} values calculated for the squirt flow model. The Q^{-1} peak could correspond to the maximum attenuation frequency peak in a standard linear solid of Zener (1948). The comparison of the obtained results on Q^{-1} with the magnitude of the attenuation predicted by a standard linear solid (e.g. Schmeling 1985; Mainprice & Ildefonse, private communication, 2000) supports the hypothesis that the melt squirt flow may be only an additional attenuation mechanism of the internal friction at high temperatures.

Faul *et al.* (2004) observed in their melt bearing samples that the melt films are ≤1 nm thick. They argued that the melt in thin films is affected by the short range Van der Waals forces from the neighbouring crystals (e.g. Hess 1994) and that a melt film is expected to have much higher shear viscosity than the bulk shear melt viscosity. They assume that it is also true in the case of the olivine–olivine grain boundaries in their melt bearing samples. Therefore, they suggested that the attenuation peak could be due to a viscous shear flow on grain boundaries. In our experiments, we observed that the melt films are significantly thicker ($\geq 1\,\mu$m). In addition, we do not observe an attenuation peak in experiments between 1050°C and 1110°C, in which the melt films could be thinner than 1 μm. It is obvious that the relaxation time of melt squirt flow and the elastically accommodated grain boundary sliding both depend on viscosity. In both cases, only a low-temperature, low-frequency shoulder of the attenuation peaks may be observed in the temperature–frequency operational window of the present experiments. Consequently, for stable microstructures, the internal friction peak being due to one of these two thermally activated processes, will move from low frequencies at low temperature to higher frequencies at higher temperature, and thus, it is difficult to distinguish the separate contribution from each of them into the resulting high temperature attenuation. However, the origin of the peak shifting in our experiments might not be directly related to these two mechanisms because the crack density and the melt fraction are also varied over the large temperature interval in the present study.

This study clearly confirms the complicated dependence of Q^{-1} on temperature and the important effect of the onset of melting. The complex dependence of Q^{-1} on temperature stems from the combination of different effects:

(1) temperature-driven attenuation mechanisms in solid phases,

(2) progressive melting and increasing melt fraction with temperature,

(3) progressive interconnection of the melt phase and disintegration of the crystalline phase,

(4) variation of the chemical composition of the melt with the progressive melting and

(5) possibly progressive mean grain size reduction due to the melting increase.

6.4 Extrapolation to crustal conditions

The present experiments were conducted at ambient pressure. The effect of the confining pressure on Q^{-1} must be determined in order to extrapolate the laboratory data to the conditions in the lower crust. At high temperatures the samples would be devoid of cracks because of better sintering and grain recrystallization under pressure. For that reason, the only pressure effect on Q^{-1} that can be evaluated is the possible pressure effect on the activation energy via thermodynamic parameters. For a diffusion-controlled mechanism, both pressure and temperature affect the activation energy via the activation volume and the activation entropy. Dresen & Rybacki (2005) estimated an activation volume of $\Delta V = 24 \pm 21$ cm^3 mol^{-1} for anhydrous anorthite samples deforming by diffusion creep. Hier-Majumder *et al.* (2005) obtained $\Delta V = 14 \pm 6$ cm^3 mol^{-1} for creep of water saturated clinopyroxenite. It can be assumed that Q^{-1} at the thermal conditions from 4 to 10 km depth is dominated by the HTB. We made an estimation of how Q^{-1} may change with depth using a correction factor $\exp(-\Delta V \cdot P/RT)^{\alpha}$. At the depth of 10 km (pressure $P \sim 0.3$ GPa) and for $T = 700^{\circ}$C, Q^{-1} decreases to 7 per cent in dry anorthite and in 4 per cent in water saturated clinopyroxenite. This increase is negligible in the logarithmic scale for interpretation of the attenuation anomalies from partially molten regions at this depth. Moreover, if ΔV is between 14 and 24 cm^3 mol^{-1}, then the correction to the activation energy at 0.3 GPa due to the pressure effect is about 4–7 kJ mol^{-1}. This correction is less than the error in the estimated activation energy from our experiments. For high temperatures ($T > 400^{\circ}$C) and lithospheric pressures ($\leq$0.5 GPa) correction for Q^{-1} are insignificant. At low temperature ($T \sim 400^{\circ}$C) and pressures $\sim$1 GPa, the pressure correction factor of Q^{-1} may be significant, *c*. 60 per cent when $\alpha \sim 0.2$ or 70 per cent, when $\alpha \sim 0.3$.

7 SUMMARY AND CONCLUSIONS

A series of six forced-oscillation experiments in a partially molten microgabbronorite at low frequencies and atmospheric pressure has been conducted, in an attempt to characterize and quantify the factors controlling Q^{-1}. After the experiments, samples were studied with optical and scanning electron microscopes to describe the texture, grain size and to estimate the melt fraction and its connectivity. These experimental results bring further constraints to plausible models of Q^{-1} in partially molten zones in magma chambers, in layers of cumulates and in melt-bearing partially molten gabbros in particular.

The main conclusions of this study may be summarized as follows:

(1) Whatever the foliation orientation with respect to the applied torque, melt is preferentially aligned in the foliation. Below melting temperature ($\sim$1050°C), the magnitude of attenuation is, to the first order, an exponentially increasing function of the reciprocal temperature, attributed to the diffusion controlled grain boundary sliding. Above the melting temperature, the magnitude of attenuation is possibly related to both the temperature dependence and the presence of a melt fraction. The first-order effect of melt fraction on Q^{-1} above melting temperature is supported by (i) the observation in thin sections, after experiments, of phases resulting from partial melting of the rock, (ii) the results of linear and multiple regression calculations, showing that the correlation with a model in which the magnitude of Q^{-1} is only weakly correlated with temperature at high temperature and (iii) the fact that Q^{-1} calculated for the squirt flow model is of the same order of magnitude as the difference between the measured Q^{-1} and the computed temperature-related (HTB) Q^{-1}. In our experiments the average crack aspect ratio is $\sim 10^{-3}$–10^{-2} and the viscosity is 310 Pa s from direct measurement of basaltic and andesitic melts viscosity (Fontaine & Neuville, in preparation, 2005). The characteristic frequency for the melt squirt flow was estimated to be $\omega_m \sim 0.15$–300 Hz for a bulk modulus of 50–90 GPa.

(2) Attenuation can be approximated by an experimental power law $Q^{-1} = A \cdot [\omega^{-1} \cdot d^{-1} \cdot \exp(-E_a/RT)]^{\alpha}$ with $\alpha \sim 0.08$, $A = 34.72\ \mathrm{s}^{-\alpha}\ \mu\mathrm{m}^{-\alpha}$, and $E_a \sim 873$ kJ mol^{-1}.

(3) The dependence of the internal friction to the grain size d is correlated with the frequency dependence of Q^{-1}. In materials with the frequency independent Q^{-1} one may expect a weak dependence of the attenuation to the grain size.

Further work on experimental texture formation, along with more accurate textural descriptions of rocks at several temperatures, is necessary in order to (1) clearly identify microstructures due to the squirt flow and (2) determine the precise critical melt fraction percentage when the framework is disaggregated by melt. A much more extended study of gabbros with varying composition and grain size would be necessary in order to properly parameterize Q^{-1} beneath mid-oceanic ridges.

ACKNOWLEDGMENTS

This work was supported by the French-German 'Programme d'Action Intégrée' Procope (# 99102) and by the French program Dorsales (# 99-01). The authors thank D. Mainprice, D. Neuville, K. Müller, J-M. Dautria, G. Barruol, D. R. Toomey, M. Godard, F. Boudier, A. Vauchez, for helpful discussions, and C. Nevado for his high-quality thin sections. We are also grateful to Y. Guéguen, I. Jackson, R. F. Cooper, U. Faul and P. Kelemen for valuable comments and reviews of the former version of this paper.

REFERENCES

Aki, K. & Richards, P.G., 1980. *Quantitative Seismology, theory and Methods*, p. 932, W. H. Freeman and Co., San Francisco.

Bagdassarov, N., 2000. Anelastic and viscoelastic behaviour of partially molten rocks and lavas, in *Physics and Chemistry of Partially Molten Rocks*, pp. 29–65, eds Bagdassarov, N., Laporte, D. & Thompson, A.B., Kluwer Academic Publishers, Dordrecht.

Bagdassarov, N.S. & Dingwell, D.B., 1993. Frequency dependent rheology of vesicular rhyolite, *J. geophys. Res.,* **98,** 6477–6487.

Berckhemer, H., Kampfmann, W., Aulbach, E. & Schmeling, H., 1982. Shear modulus and *Q* of forsterite and dunite near partial melting from forced-oscillation experiments, *Phys. Earth planet. Int.,* **29,** 30–41.

Bottinga, Y. & Weill, D.F., 1972. The viscosity of magmatic silicate liquids, a model calculation, *American Journal of Science,* **272,** 438–475.

Boudier, F., Godard, M. & Armbruster, C., 2000. Significance of gabbronorite occurence in the crustal section of the Semail ophiolite, *Marine Geophys. Res.,* **21,** 307–326.

Bulau, J.R., Waff, H.S. & Tyburczy, J.A., 1979. Mechanical and thermodynamic constraints on fluid distribution in partial melts, *J. geophys. Res.,* **84,** 6102–6108.

Cmíral, M., Fitz Gerald, J.D., Faul, U.H. & Green, D.H., 1998. A close look at dihedral angles and melt geometry in olivine-basalt aggregates: a TEM study, *Contrib. Mineral. Petrol.,* **130,** 336–345.

Cox, K.G., Bell, J.D. & Pankhurst, R.J., 1979. *The interpretation of Igneous Rocks*, p. 445, George Allen & Unwin, London.

Dahl, R., 1984. Etude géométrique, pétrologique et géochimique de la séquence crustale de l'ophiolite d'Oman, Massif de Rustaq (bloc d'Haylayn). Un modèle tridimensionnel de zone d'accrétion, *PhD thesis,* Université de Clermont-Ferrand, Clermont-Ferrand, p. 264.

Dimanov, A., Dresen, G. & Wirth, R., 1998. High-temperature creep of partially molten plagioclase aggregates, *J. geophys. Res.,* **103,** 9651–9664.

Dimanov, A., Dresen, G., Xiao, X. & Wirth, R., 1999. Grain boundary diffusion creep of synthetic anorthite aggregates: The effect of water, *J. geophys. Res.,* **104,** 10 483–10 497.

Dortman, N.B., 1976. Fiziceskie svoistva gornich porod i polesnich iskopamych, Izdat. Nedra, Moskva.

Dresen, G. & Rybacki, E., 2005. Strength estimates of the lower crust from the view from the laboratory, *Geophys. Res. Abstr.,* **7,** 04587.

Faul, U.H., Fitz Gerald, J.D. & Jackson, I., 2004. Shear-wave attenuation and dispersion in melt-bearing olivine polycrystals II. Microstructural interpretation and seismological implications, *J. geophys. Res.,* **109,** B06202, doi:10.1029/2003JB002407.

Findley, W.N., Lai, J.S. & Onaran, K., 1976. *Creep and Relaxation of Nonlinear Viscoelastic Materials*, p. 368, North-Holland Publishing Company, Amsterdam.

Gebrande, H., Kern, H. & Rummel, F., 1982. Elasticity and Inelasticity, in *Landolt-Börnstein Numerical Data and Functional Relationships in Science and Technology*, Vol. 1, ed. Hellwege, K.-H., New Series; Group V. Geophysics and Space Research, Physical Properties of Rocks, Subvolume b, 1–223. Springer-Verlag, Berlin.

Gribb, T.T. & Cooper, R.F., 1998. Low-frequency shear attenuation in polycristalline olivine: grain boundary diffusion and the physical significance of the Andrade model for viscoelastic rheology, *J. geophys. Res.,* **103,** 27 267–27 279.

Guéguen, Y., Woigard, J. & Darot, M., 1981. Attenuation mechanisms and anelasticity in the upper mantle, in *Anelasticity in the Earth*, pp. 86–94, eds Stacey, F.D., Paterson, M.S. & Nicholas, A., American Geophysical Union, Washington DC.

Guéguen, Y., Darot, M., Mazot, P. & Woirgard, J., 1989. Q^{-1} of forsterite single crystals, *Phys. Earth planet. Inter.,* **55,** 254–258.

Hammond, W.C. & Humphreys, E.D., 2000. Upper mantle seismic wave attenuation: effects of realistic partial melt distribution, *J. geophys. Res.,* **105,** 10 987–10 999.

Hess, P.C., 1994. Thermodynamics of thin fluid films, *J. geophys. Res.,* **99,** 7219–7229.

Hier-Majumder, S., Mei, S. & Kohlstedt, D.L., 2005. Water weakening of clinopyroxenite in diffusion creep, *J. geophys. Res.,* **110,** B02202, doi:10.1029/2004JB003292.

Hunter, R.H., 1987. Textural equilibrium in layered igneous rocks. in *Origins of Igneous Layering*, pp. 473–503, ed. Parsons, I., Dordrecht, Reidel.

Jackson, I., 2000. Laboratory measurement of seismic wave dispersion and attenuation: recent Progress, in *Earth's Deep Interior: Mineral Physics and Tomography From the Atomic to the Global Scale*, pp. 265–289, eds Karato, S.I., Forte, A.M., Liebermann, R.C., Masters, G. & Stixrude, L., Geophysical Monograph 117, American Geophysical Union, Washington DC.

Jackson, I., Gerald, J.D.F. & Kokkonen, H., 2000. High-temperature viscoelastic relaxation in iron and its implications for the shear modulus and attenuation of the Earth's inner core, *J. geophys. Res.,* **105,** 23 605–23 634.

Jackson, I., Gerald, J.D.F., Faul, U.H. & Tan, B.H., 2002. Grain-size sensitive seismic-wave attenuation in polycrystalline olivine, *J. geophys. Res.,* **107**(B12), 2360, doi:10.1029/2001JB001225.

James, M.R., Bagdassarov, N., Müller, K. & Pinkerton, H., 2004. Viscoelastic behaviour of basaltic lavas, *J. Volc. Geotherm. Res.,* **132,** 99–113.

Ji, S., 1987. Déformation plastique naturelle et expérimentale des plagioclases, *PhD thesis,* Université des Sciences et Techniques du Languedoc, Montpellier, p. 222.

Johnston, D.H. & Toksöz, M.N., 1980. Thermal cracking and amplitude dependent attenuation, *J. geophys. Res.,* **85,** 937–942.

Kampfmann, W. & Berckhemer, H., 1985. High temperature experiments on the elastic and anelastic behavior of magmatic rocks, *Phys. Earth planet. Int.,* **40,** 223–247.

Karato, S. & Spetzler, H.A., 1990. Defect microdynamics in minerals and solid-state mechanisms of seismic wave attenuation and velocity dispersion in the mantle, *Rev. Geophys.,* **28,** 399–421.

Longhi, J. & Jurewicz, S.R., 1995. Plagioclase-melt wetting angles and textures: implications for anorthosites, *Lunar and Planetary Sciences,* **26,** 859–860.

Mainprice, D., 1997. Modelling the anisotropic seismic properties of partially molten rocks found at mid-ocean ridges, *Tectonophysics,* **279,** 161–179.

Mavko, G.M. & Nur, A., 1975. Melt squirt in the asthenosphere, *J. geophys. Res.,* **85,** 5173–5189.

Mavko, G.M., Mukerji, T. & Dvorkin, J., 1998. *The Rock Physics Handbook. Tools for Seismic Analysis in Porous Media*, pp. 329, Cambridge University Press, Cambridge.

Montardi, Y., 1987. Etude du frittage et de la déformation plastique expérimentale de plagioclases, *PhD thesis,* Université des Sciences et Techniques du Languedoc, Montpellier, France, p. 249.

Nowick, A.S. & Berry, B.S., 1972. *Anelastic Relaxation in Crystalline Solids*, p. 678, Academic Press, London.

O'Connell, R.J. & Budiansky, B., 1977. Viscoelastic properties of fluid-saturated cracked solids, *J. geophys. Res.,* **82,** 5719–5735.

Pezzotti, G., 2003. Mechanical spectroscopy methods for the quantitative analysis of intergranular glass viscosity in polycrystalline ceramics, *Journal of Non-Crystalline Solids,* **321,** 37–51.

Rybacki, E. & Dresen, G., 2000. Dislocation and diffusion creep of synthetic anorthite aggregates, *J. geophys. Res.,* **105,** 26 017–26 036.

Sato, H. & Ida, Y., 1984. Low frequency electrical impedance of partially molten gabbro: the effect of melt geometry on electrical properties, *Tectonophysics,* **107,** 105–134.

Schmeling, H., 1985. Numerical models on the influence of partial melt on elastic, anelastic and electric properties of rocks. Part I: elasticity and anelasticity, *Phys. Earth planet. Int.,* **41,** 34–57.

Shaw, H.R., 1972. Viscosities of magmatic silicate liquids: an empirical method of prediction, *Am. J. Sci.,* **272,** 870–893.

Tan, B.H., Jackson, I., & Gerald, J.D.F., 2001. High-temperature viscoelasticity of fine-grained polycrystalline olivine, *Phys. Chem. Minerals,* **28,** 641–664.

Tselentis, G.A., 1998. Intrinsic and scattering seismic attenuation in W. Greece, *Pure appl Geophys.,* **153,** 703–712.

Wang, Z., Dresen, G. & Wirth, R., 1996. Diffusion creep of fine-grained polycrystalline anorthite at high temperature, *Geophys. Res. Let.,* **23,** 3111–3114.

Wark, D.A., Williams, C.A., Watson, E.B. & Price, J.D., 2003. Reassessment of pore shapes in microstructurally equilibrated rocks, with implications for permeability of the upper mantle, *J. geophys. Res.,* **108**(B1), 2050, doi:10,1029/2001JB001575.

Zener, C., 1948. *Elasticity and Anelasticity of Metals*, p. 163, University of Chicago Press, Chicago.